JOURNAL OF MECHANICAL ENGINEERING AND SCIENCES
ISSN: 2289-4659 e-ISSN: 2231-8380
VOLUME 17, ISSUE 3, 2023, 9637 – 9655
DOI: https://doi.org/10.15282/jmes.17.3.2023.9.0763

UNIVERSITI MALAYSIA PAHANG AL-SULTAN ABDULLAH

RESEARCH ARTICLE

Vibrations control of railway vehicles using decentralized proportional integral derivative controller with flow direction optimization algorithm

Nitish, A. K. Singh*

Department of Instrumentation and Control of Engineering, Dr. B. R. Ambedkar National Institute of Technology, Jalandhar, Punjab, 144008, India
Phone: +01815037681-2912

ABSTRACT - The reduction of vibration-induced discomfort in vehicles is an important goal in the field of transportation engineering. Several mathematical models with various controlling techniques, from classical to modern, have been employed to achieve better ride comfort. Still, no comprehensive solution has yet been found. Therefore, this paper proposes a 17-degree-of-freedom (minimum number of coordinates) dynamic model of a full-scale railway vehicle integrated with wheel-rail contact forces and an active suspension system. Two controllers, termed system and force tracking controllers, suppress the vehicle body's vibrations. Based on a multi-loop control structure, three optimally tuned Proportional Integral Derivative controllers evaluate the desired control forces and performs the system controller's action. While the force-tracking controller generates the command voltage to track that forces. The parameters of controllers are tuned with a novel metaheuristic optimization algorithm known as the flow direction algorithm (FDA), and the results are compared with two other optimization techniques, i.e., particle swarm optimization and ant colony optimization. The simulated results show that the ride comfort of the vehicle is improved with FDA, as the root mean square values of the lateral, roll, and yaw accelerations are reduced by 42.01%, 33.12%, and 48.24%, respectively. Moreover, the simulated results of the proposed model are validated with the experimental results of accelerations. The simulated results show that the proposed system tuned with the metaheuristic algorithm outperforms with a significant reduction in vehicle vibrations.

ARTICLE HISTORY
Received : 08th May 2023
Revised : 19th Aug. 2023
Accepted : 29th Aug. 2023
Published : 28th Sept. 2023

KEYWORDS
Active suspension system
Electro-hydraulic actuator
Flow direction algorithm
Multi-loop control structure
Proportional integral derivative controller
Power spectral densities

1.0 INTRODUCTION

Over the past few decades, the railway industries have concentrated on increasing train speed while enhancing travel comfort and safety. However, faster trains and the presence of track abnormalities will significantly raise the vibration level, lowering the stability and pleasure of the trip. To improve ride comfort and safety, vehicle vibrations must be reduced. Two approaches can be used to address these vibration issues: improving the state of the railway tracks and improving the vibration mitigation system. Since the track cannot be altered once built, the second strategy of improving vibration mitigation systems is more practicable. The car suspensions have three vibration mitigation systems: passive, semi-active, and active [1]. A passive system comprises basic and low-cost static springs and oil/pneumatic dampers. Despite its low cost and simple design, the passive system does not deliver acceptable control performances in ride comfort or quality [2]. On the other hand, a semi-active system is outfitted with a variable gain damper filled with a rheological fluid whose viscosity changes when exposed to an electric or magnetic field. Electro-rheological (ER) and Magneto-rheological (MR) fluids are utilized in semi-active suspension and are responsible for variable damping [3, 4]. Previous research articles have discussed using ER and MR fluid in semi-active suspension to minimize vibrations [5–10]. The MR-based damper is the most successful because it generates more power and has a more comprehensive operating temperature range than an ER damper. However, a semi-active suspension system's complex control techniques make it difficult to suppress vibrations successfully across the broad frequency range [11,12]. Thus, researchers discovered an alternate vibration control method in the form of active suspension by realizing the limitations of both passive and semi-active systems [13]. Hence, this paper investigates the performance of an active suspension system that mitigates the car body's vibrations and enhances the ride comfort of railway vehicles.According to previous research, an active suspension system combines the passive components with controller-controlled actuators that generate extra force. It can continually reduce the vibrations of the vehicle over a wide range of frequencies and provide better ride comfort [14,15]. Using various control structures and algorithms, the system controller calculates the extra force required to suppress the vibrations. Several research papers on traditional and modern controllers to maximize the performance of active suspension systems have been published. These include the use of proportional integral derivative (PID) control [16–22], fuzzy logic control [23, 24], sliding mode control [25, 26], neuro-fuzzy control [27], model predictive control [28, 29], optimal &H_∞control [30-33] and neural-network-based control [34–36]. Among them, the proportional integral derivative controller is still a favorite in modern control domains because of its simple and robust performance under various operating situations. The PID controller's performance is determined by the values of three parameters, K_P, K_i, and K_d, which must be optimally tuned according to the desired output. The traditional tuning methods such as Ziegler-

***CORRESPONDING AUTHOR | A. K. Singh** | ✉ singhak@nitj.ac.in

Nichols (Z-N) [38] and Cohen-Coon [39], which were previously thought to be the best, are now being supplemented by heuristic optimization techniques because traditional methods may fail to provide the desired performance in terms of overshoot, settling time, and steady-state error.

The parameters calculated from the classical method could not give the optimum value of the PID controller. This is mainly because these processes could not provide a fully protected space in terms of data, which helps in achieving the minimum value of cost function. Thus, the intellectual methods based on metaheuristic algorithms are promising approaches to enhance search accuracy. These algorithms can learn much faster as they operate. The main objective of these intellectual methods is to minimize the cost function depending on the performance of algorithms. The performance of these metaheuristic algorithms is highly efficient in solving complex optimization problems. Several types of evolutionary algorithms, such as genetic algorithm [40], particle swarm optimization (PSO) [41], ant colony optimization (ACO) [42], grey wolf optimization [43], firefly algorithm [44], cuckoo search algorithm [45], flow direction algorithm (FDA) [46], are generally used as intelligent optimizers to solve any dynamic problems. For instance, El-Deen et al. [47] and Mohammed et al. [48] used a genetic-based algorithm to tune the PID for speed control of the dc motor and the generators' synchronization.

The successful implementation of particle swarm and ant colony optimization for automatic voltage regulator systems has been reported in [49] and [50], respectively. Adubi and Misra [51] use ant colony optimization in various applications, and a comparative study is presented. The implementation of particle swarm optimization-based PID for locating the camera position in the unmanned aerial vehicle and controlling an inverted pendulum has been successfully reported by Rajesh et al. in [52] and Joseph et al. in [53]. Mahdieh Alamdar et al. [54] proposed a chaotic firefly algorithm to tune the parameters of fractional order-PID for a continuous stirred tank reactor. The cuckoo search algorithm has been used to optimize the PID parameters for various applications such as maximum power point tracking [55], speed control of induction motors [56], and LED driver circuits as buck booster converters [57]. Apart from these, Li et al. Proposed grey wolf optimization for condenser pressure control using a PI controller [58]. Yadav et al. used this algorithm to tune the parameters of PID used for the magnetic levitation system [59]. Laith Abualigah et al. [60] used FDA to solve the optimization problem of data clustering, and Pati et al. [61] used this algorithm to minimize the energy consumption of multi-stage evaporators used in the pulp industry.

According to the literature, PID controllers tuned with meta-heuristic optimization have been employed for various applications, including chemical processes, motor speed control, sun tracking systems, vibration control, voltage regulation systems, and many more. However, few studies on PID have been published in the context of vibration control employing an active suspension system. Moreover, for a multi-input multi-output system, two types of control structures, i.e., centralized and decentralized, are reported in the literature [62]. Whereas most of the research has been carried out using a centralized control structure, this creates the problem of a large amount of data transmission at one time and makes the system complex. A decentralized or multi-loop control technique, which also has a basic structure, can be used to solve the problem of massive data transfer [63, 64].

As per the contribution of this paper, the following points are worth noting. First, a 17-degree-of-freedom dynamic model of a full-scale railway vehicle completed with wheel-rail forces and active suspension is developed. The system's performance is evaluated under lateral alignment, and cross-level type of random track irregularities. Then, a multi-loop control structure with three independent system controllers is used to suppress the vibration of the car body's lateral, roll, and yaw motion. A novel metaheuristic optimization technique, FDA, is proposed to tune the PID controller, and the results are compared with two other optimization algorithms, i.e., PSO and ACO. Based on the objective function, the proposed optimization techniques are used to determine the desired force through the system controller. The required amount of force is delivered with the help of the electro-hydraulic actuator controlled by a force-tracking controller. The results of optimized PID are critically analyzed in the frequency domains and represented in terms of power spectral densities. Finally, the pursuit of the proposed system is validated with the experimental results.

2.0 ANALYTICAL MODEL

This section presents the dynamic railway vehicle model, state space, and random track irregularities model.

2.1 Dynamic Model of a Railway Vehicle

The dynamic motion of the car body, bogies, and wheel-set of a railway vehicle with wheel-rail interaction has been described with the governing equations of motion. The definitions of various symbols used in dynamic modeling have been given in Table 1. The pictorial representations are given in Figures 1. The governing equation of motion of railway vehicle dynamics is presented as follows [7]:

Car body dynamics:

$$M_c \ddot{Y}_c + 2K_{2y}[2(y_c + h_3\theta_c) - y_{t1} - y_{t2} - h_2\theta_{t1} - h_2\theta_{t2}] + 2C_{2y}[2(\dot{y}_c + h_3\dot{\theta_c}) - \dot{y}_{t1} - \dot{y}_{t2} - h_2\dot{\theta}_{t1} - h_2\dot{\theta}_{t2}] = [F_{y1} + F_{y2}] \quad (1)$$

$$I_{Xc}\ddot{\theta}_c + 2b_2^2K_{2z}(2\theta_c - \theta_{t1} - \theta_{t2}) + 2b_2^2c_{2z}\left(2\dot{\theta}_c - \dot{\theta}_{t1} - \dot{\theta}_{t2}\right) + 2h_3K_{2y}\{2(y_c + h_3\theta_3) - y_{t1} - y_{t2} + h_2\theta_{t1} + h_2\theta_{t2}) + 2h_3c_{2y}(2\left(\dot{y}_c + h_3\dot{\theta_3}\right) - \dot{y}_{t1} - \dot{y}_{t2} + h_2\dot{\theta}_{t1} \mp \dot{\theta}_{t2}] = [h_3\left(F_{y1} + F_{y2}\right)] \quad (2)$$

$$I_{Zc}\ddot{\Psi}_c + 2L_bK_{2y}(2L_b\Psi_c - y_{t1} + y_{t2} - h_2\theta_{t1} + h_2\theta_{t2}) + 2L_bC_{2z}\left(2\mathrm{L_b}\dot{\Psi}_c\text{-}\dot{\mathrm{y}}_{\mathrm{t1}}\text{+}\dot{\mathrm{y}}_{\mathrm{t2}}\text{-}\mathrm{h_2}\dot{\theta}_{\mathrm{t1}}\text{+}\mathrm{h_2}\dot{\theta}_{\mathrm{t2}}\right) + \quad 2d_sK_{2x}(2\Psi_c - X_{t1} - X_{t2}) = L_b[F_{y1} - F_{y2}] \quad (3)$$

Bogie dynamics (i=1, 2):

$$M_t\ddot{y}_{ti} + 2c_{1y}\left[2\dot{y}_{ti} - \left(\dot{y}_{w(2i-1)} + \dot{y}_{w(2i)}\right) + 2h_1\dot{\theta}_{ti}\right] + 2c_{2y}\left[\left(\dot{y}_{ti} - \dot{y}_{w(2i-1)}\right) - \left(h_3\dot{\theta}_c + h_2\dot{\theta}_{ti}\right) - (-1)^iL_b\dot{\Psi}_c\right] + 2k_{1y}\left[2y_{ti} - \left(y_{w(2i-1)} + y_{w(2i)}\right) + 2h_1\theta_{ti}\right] + 2k_{2y}[(y_{ti} - y_c) - (h_3\theta_c + h_2\theta_{ti}) - (-1)^iL_b\Psi_c] = -F_{yi} \quad (4)$$

$$J_{xt}\ddot{\theta}_{ti} + 2h_1c_{1y}\left[2h_1\dot{\theta}_{ti} + \left(2\dot{y}_{ti} - \left(\dot{y}_{w(2i-1)} + \dot{y}_{w(2i)}\right)\right)\right] + 2h_2c_{2y}\left[h_3\dot{\theta}_c + h_2\dot{\theta}_{ti} + (\dot{y}_{ti} + \dot{y}_c) - (-1)^iL_b\dot{\Psi}_c\right] + 2b^2{}_1c_{1z}\left[2\dot{\theta}_{ti} - \left(\dot{\theta}_{w(2i-1)} + \dot{\theta}_{w(2i)}\right)\right] + 2b^2{}_2c_{2z}\left[\dot{\theta}_{ti} - \dot{\theta}_c\right] + 2h_1k_{1y}\left[2h_1\theta_{ti} + \left(2Y_{ti} - \left(Y_{w(2i-1)} + Y_{w(2i)}\right)\right)\right] + 2h_2k_{2y}[h_3\theta_c + h_2\theta_{ti} + (Y_{ti} + Y_c) - (-1)^iL_b\Psi_c] + 2b^2{}_1k_{1z}\left[2\theta_{ti} - \left(\theta_{w(2i-1)} + \theta_{w(2i)}\right)\right] + 2b^2{}_2k_{2z}[\theta_{ti} - \theta_c] = -F_{yi}h_3 \quad (5)$$

$$J_{Zt}\ddot{\Psi}_{ti} + 2d^2{}_pc_{1x}\left[2\dot{\Psi}_{ti} - \left(\dot{\Psi}_{w(2i-1)} + \dot{\Psi}_{w(2i)}\right)\right] + 2L_dc_{1y}\left[2L_d\dot{\Psi}_{ti} - \left(\dot{Y}_{w(2i-1)} - \dot{Y}_{w(2i)}\right)\right] + 2d^2{}_pk_{1x}\left[2\Psi_{ti} - \left(\Psi_{w(2i-1)} + \Psi_{w(2i)}\right)\right] + 2d^2{}_sk_{2x}[\Psi_{ti} - \Psi_c] + 2L_dk_{1y}\left[2L_d\emptyset_{ti} - \left(Y_{w(2i-1)} - Y_{w(2i)}\right)\right] = 0 \quad (6)$$

Table 1. Various symbols used in the modeling (where $\boldsymbol{i}$ = 1,2 & $\boldsymbol{j}$ = 1,2,3,4)

Symbols	Definitions
Y_c , Y_{ti} , Y_{wj}	Lateral displacement of the car body, bogies, and wheel-sets
Ψ_c , Ψ_{ti} , Ψ_{wj}	Yaw displacement of the car body, bogie, and wheel-sets
Θ_c , Θ_{ti}	Roll displacement of the car body, bogie
F_{yi}	Lateral control forces
$\mathrm{Y_{rj}}$,θ_{clj}	Rail track disturbances

Wheel-set dynamics (i=1,2, while$j$=1; i=3,4, while$j$=2):

$$M_w\ddot{y}_{wi} + 2c_{1y}\left[\left(\dot{Y}_{wi} - \dot{Y}_{tj}\right) - h_1\dot{\theta}_{tj} + L_d\dot{\Psi}_{tj}\right] + 2k_{1y}\left[\left(Y_{wi} - Y_{tj}\right) - h_1\theta_{tj} + L_d\dot{\Psi}_{tj}\right] + k_{hy}[Y_{wi} - Y_{ai}] + \quad 2f_{22}\left[\frac{1}{V}\left(1 + \frac{\sigma R_1}{a}\right)\dot{Y}_{wi} - \frac{\sigma R_1}{V a}\dot{Y}_{ai} - \frac{\sigma {R_1}^2}{V a}\dot{\theta}_{cli} - \Psi_{wi}\right] = 0 \quad (7)$$

$$J_{Zw}\ddot{\Psi}_{wi} + 2d_p^2c_{1x}\left[\left(\dot{\Psi}_{wi} - \dot{\Psi}_{tj}\right)\right] + 2d_p^2k_{1x}\left[\Psi_{wi} - \Psi_{tj}\right] + 2f_{11}\left[\frac{\lambda_e a}{R_1}(Y_{wi} - Y_{ai} - R_1\theta_{cli}) + \frac{a^2}{V}\dot{\Psi}_{wi}\right] + k_{gy}\Psi_{wi} = 0 \quad (8)$$

The definitions and values of various parameters used in Eqs. (1) – (8) are the same as in [22, 65]. The state space formulation of the above system has been given in the next section.

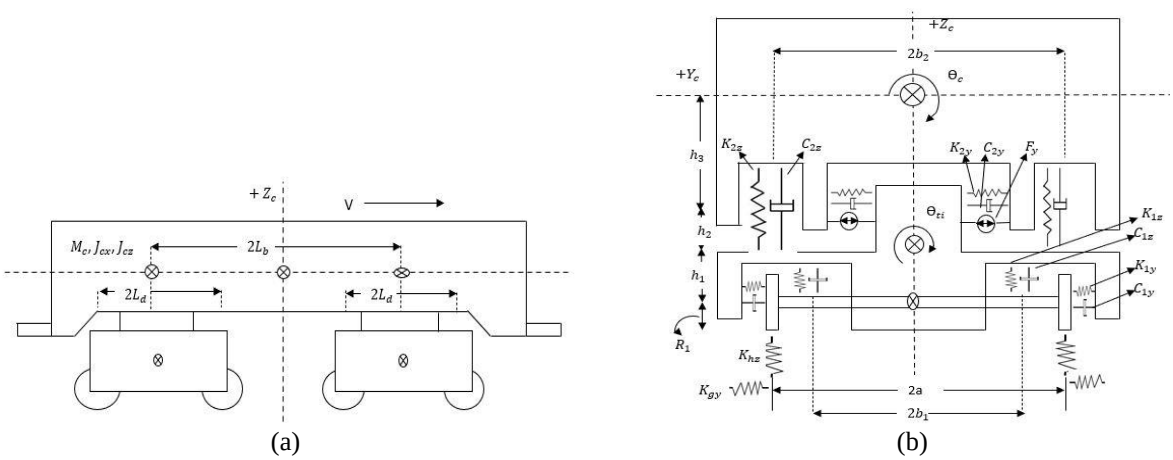

(a) (b)

Figure 1. 17-DOF analytical model of a railway vehicle: (a) end view, (b) front view

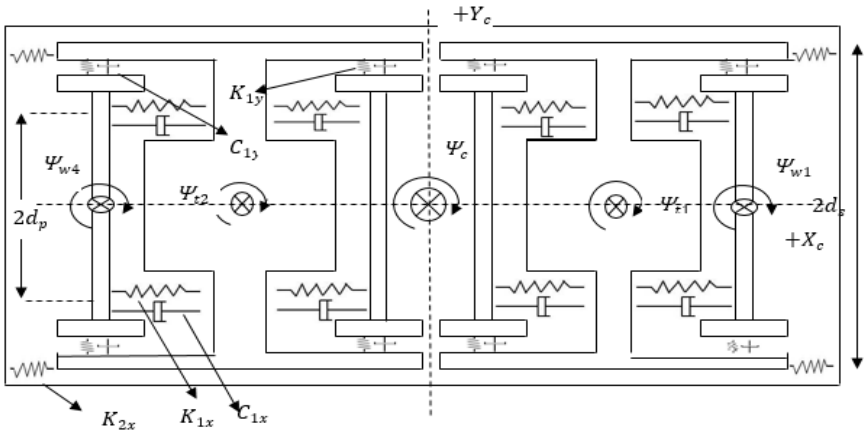

(c)

Figure 1. (cont.) top view

2.2 State-Space Formulation

In this section, the state-space modeling of railway vehicle is presented.

Let,

$q = [Y_c, \Theta_c, \psi_c, Y_{t1}, \Theta_{t1}, \psi_{t1}, Y_{t2}, \Theta_{t2}, \psi_{t2}, Y_{w1}, \psi_{w1}, Y_{w2}, \psi_{w2}, Y_{w3}, \psi_{w3}, Y_{w4}, \psi_{w4}]^{\mathrm{T}}$,$u = [\, F_{y1}, F_{y2}]^{\mathrm{T}}$,
and $w = [Y_{a1},\ \theta_{cl1},\ Y_{a2},\ \theta_{cl2},\ Y_{a3},\ \theta_{cl3},\ Y_{a4},\ \theta_{cl4},\ \dot{Y}_{a1}, \dot{\theta}_{cl1},, \dot{Y}_{a2},\ \dot{\theta}_{cl2}, \dot{Y}_{a3},\ \dot{\theta}_{cl3},\ \dot{Y}_{a4},\ \dot{\theta}_{cl4}]^{\mathrm{T}}$
be defined the displacements (linear and angular), control, and disturbance vectors, respectively.

Then the equations of motion, represented by the Eqs. (1) - (8) can be written in the following matrix form:

$$[M]\ddot{q} + [C]\dot{q} + [K]q = [F_u]u + [F_w]w \tag{9}$$

where [M] ($\mathcal{R}^{17\times17}$), [C] ($\mathcal{R}^{17\times17}$), and [K] ($\mathcal{R}^{17\times17}$) are the mass, damping, and stiffness matrices of the vehicle system;$[F_u](\mathcal{R}^{17\times2})$, $[F_w](\mathcal{R}^{17\times16})$ are the position matrices of control inputs and track disturbances acting on the railway vehicle body and wheels of wheel-sets, respectively.

Now by defining the state vector as $\dot{x} = [q^{\mathrm{T}}\dot{q}^{\mathrm{T}}]^{\mathrm{T}}$, the state and output equations of the railway vehicle system in the

$$\begin{cases} \dot{x} = [A]\, x + [B_1]\, u + [B_2]\, w \\ y = [C]\, x + [D_1]\, u + [D_2]\, w \end{cases} \tag{10}$$

form of state-space are given as:

where$[A] = \begin{bmatrix} 0 & \mathrm{I} \\ -M^{-1}K & -M^{-1}C \end{bmatrix} \in \mathcal{R}^{34\times34}$, $[B_1] = \begin{bmatrix} 0 \\ M^{-1}F_u \end{bmatrix} \in \mathcal{R}^{34\times2}$, and $[B_2] = \begin{bmatrix} 0 \\ M^{-1}F_w \end{bmatrix} \in \mathcal{R}^{34\times16}$, are the system, control, and disturbances matrices, respectively. $[C] = [-M^{-1}K \quad -M^{-1}C] \in \mathcal{R}^{17\times34}$ is the output matrix, with $[D_1] = [M^{-1}F_u] \in \mathcal{R}^{17\times2}$, and $[D_2] = [M^{-1}F_w] \in \mathcal{R}^{17\times16}$are the transfer matrices, respectively. The values of all coefficient matrices can be derived from Eq. (9).

3.0 TRACK IRREGULARITIES

The leading cause of vibrations in the railway's vehicle body is irregularities on railway tracks and wheel structure. These irregularities act as input excitation to the railway vehicle. There are two types of track irregularity, such as lateral alignment (Y_a) and cross-level (θ_{cl})are defined in the literature [66], which excite the vehicle's body in lateral directions. These irregularities can be periodic as well as random in nature.

3.1 Random Track Irregularities

The actual track irregularities are the superposition of harmonic waves of different amplitude, phase, and wavelength. Describing the random track irregularities is always convenient in the form of PSD (power spectral density), as given in Eqs. (11) - (12), which are calculated by taking the Fourier Transform of the autocorrelation function as:

$$S_a(\omega) = \frac{A_a\,.\,\Omega_c^2\,.\,V^3}{(\omega^2+(V.\ \Omega_r)^2)(\omega^2+(V.\ \Omega_c)^2)} \frac{m^2}{(\frac{rad}{sec})} \tag{11}$$

$$S_{cl}(\omega) = \frac{A_v\,.\,\Omega_c^2\,.V^3.\ \omega^2}{l_r^2(\omega^2+(V.\ \Omega_r)^2)(\omega^2+(V.\ \Omega_c)^2)(\omega^2+(V.\ \Omega_s)^2)} \frac{m^2}{(\frac{rad}{sec})} \tag{12}$$

where ω is the angular frequency of the track measured in *rad/sec* and Ω_r, Ω_c and Ω_s are the cut-off frequencies taken in rad/m; A_v, A_a are roughness constant taken in $m^2.\frac{rad}{m}$; $V$is the velocity of the vehicle; l_r is half the distance between the two-rolling circle of the wheel-set (m) as given [22]. While the values of constant factors and cut-off frequencies for different track classes are given in Table 2.

4.0 DYNAMICS OF ELECTRO-HYDRAULIC ACTUATOR

An essential component of any active suspension system is an actuator. It is the mechanism by which the external force is injected into the system, complementing the passive suspension system. Three major actuation systems are reported in the literature [67]: Electro-hydraulic, Electro-pneumatic, and Electro-magnetic. The electro-hydraulic actuator is best suited among other actuation systems because of its excellent force/size ratio, good bandwidth, and reliability.Electro-hydraulic actuation system combines electrical and mechanical means to generate the required force, as shown in Figure 2. The primary stage of the actuation system contains an electrical motor that provides the torque according to the current value, and a hydraulic cylinder connected to the throttle spool-valve serves as a secondary stage. The position of the spool valve is controlled with motor torque, and accordingly, the controlled oil flows into the cylinder, which ultimately generates the force.

Table 2. Roughness coefficients and cut-off frequencies for German track irregularities PSDs

Track class	Ω_c (rad/m)	Ω_c (rad/m)	Ω_c (rad/m)	A_a (m^2. rad/m)	A_v(m^2. rad/m)
Low	0.8246	0.0206	0.4380	2.119×10^{-7}	4.032×10^{-7}

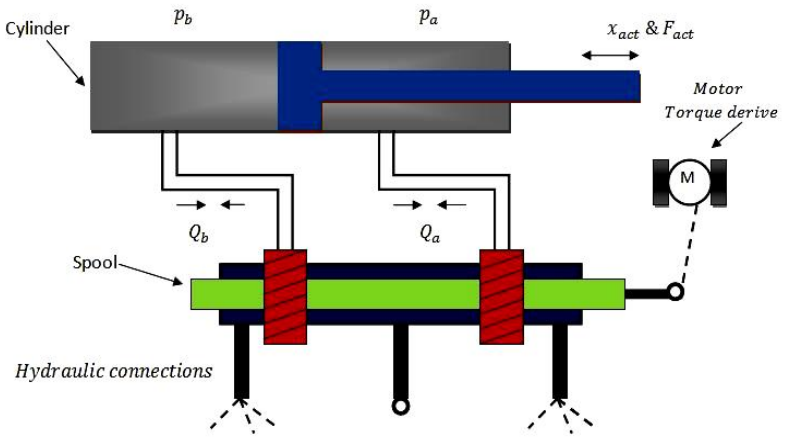

Figure 2. Electro-hydraulic actuator

Now the relation between the actuation force and motor torque may be described as:

$$F_{act} = \frac{k_i.\ i}{m_s s^2 + c_s s + k_s} \tag{13}$$

where F_{act} is the output force for an input current, i. To achieve the desired force, a force feedback control loop is required. A standard PID controller (named a force tracking controller) tune with Ziegler Nicholas is used for this. The various parameters of the electro-hydraulic actuator, used for simulation purposes, have been taken from [68]. The closed-loop control loop and the actuator's performance are shown in Figures 3 and 4, respectively. Figure 4(a) shows the actuator's ability to follow the maximum of 2000 N random force input, whereas Figure 4(b) shows the applied voltage given by the controller to track the desired force.

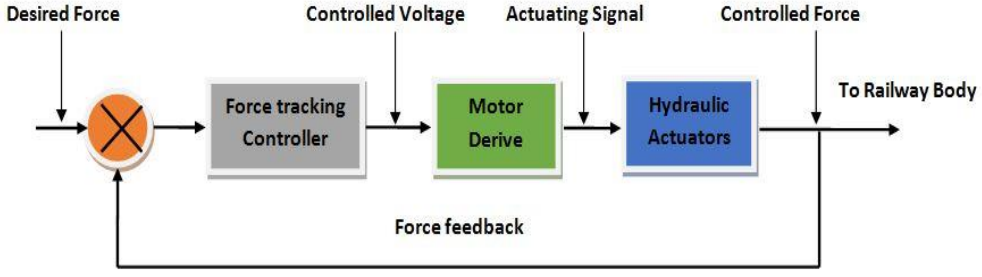

Figure 3. Control loop of the electro-hydraulic actuator

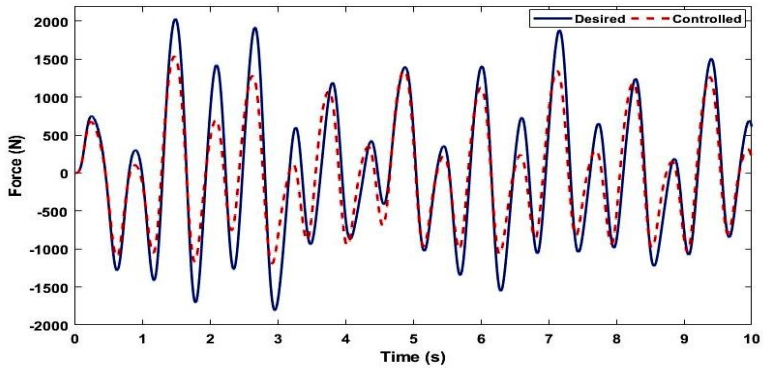

(a)

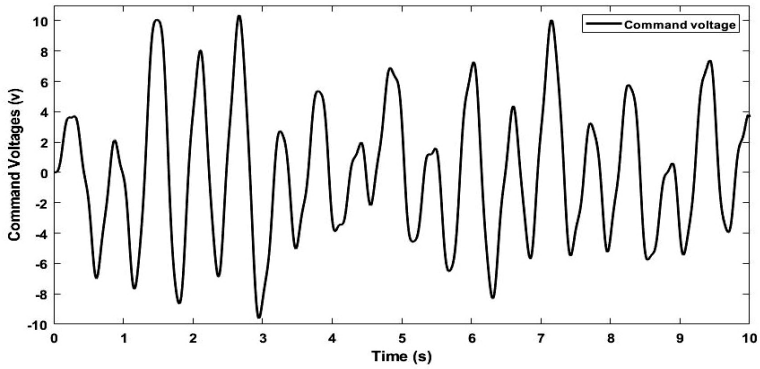

(b)

Figure 4. Validation of actuator performance (a) desired and controlled force (b) command voltage

4.1 Active Control Structure for Railway Vehicle

In this paper, a multi-loop or decentralized control structure is developed to suppress the vibrations of the railway vehicle, as illustrated in Figure 5. From the Figure 5, the points are worth noting that the developed control structure constitutes two types of controllers: the system controller and the force tracking controller. The system controllers are three optimally tuned PID controllers used to generate the desired controlling force to control the vehicle body's lateral, roll, and yaw motion. On the other hand, the force-tracking controller generates the desired voltage to track the required controlling force. Based on the error and command signal, the three body motions are controlled by implementing the two electro-hydraulic actuators above the front and rear bogies.

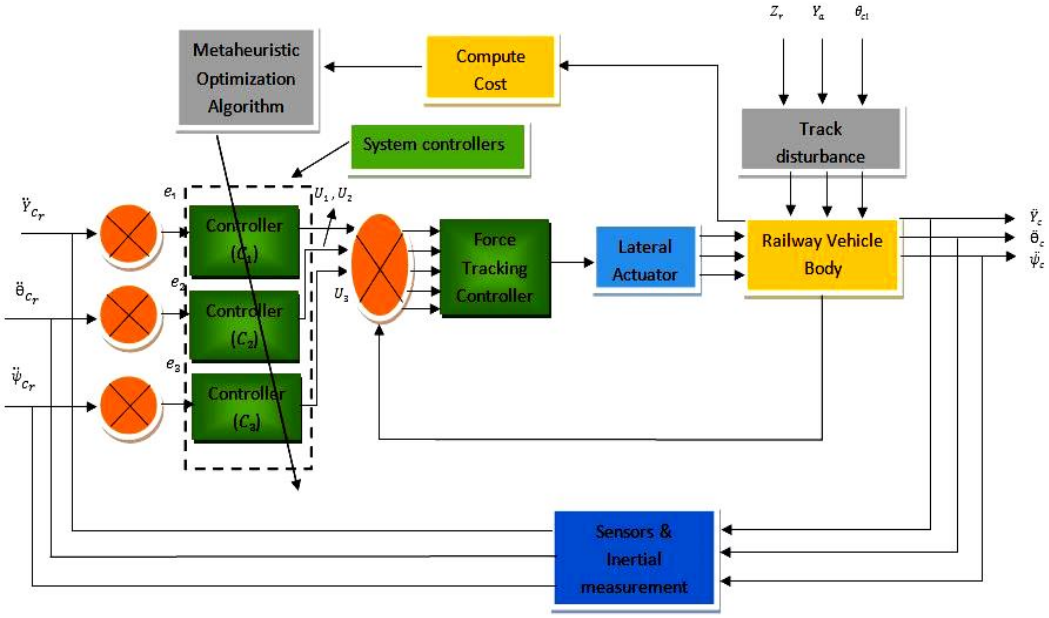

Figure 5. Decentralized control structure for railway vehicle

5.0 SYSTEM CONTROLLER AND OPTIMIZATION ALGORITHMS

This section presents the description of the proposed PID controller and the different algorithms used to tune the controller parameters.

5.1 PID Controller

The most popular and widely recognized control algorithm for industrial control is proportional-integral-derivative control. Over the years, the applications of PID controllers have shown a significant impact in the field of Engineering. Its applications in control engineering have attracted many researchers because of its robust performance and simple operation over a wide range of operating conditions. As the name suggests, the PID controller consists of three parametersK_P,K_I, and K_D, generally termed proportional, integral, and derivative constants. These three values of the controller can also be interpreted in terms of time, where K_P depends on the present, K_I depends on the future, and K_D depends on the past values of error. The fundamental equation of PID can be expressed as:

$$U(t) = K_P e(t) + K_I \int e(t) + K_D \frac{de(t)}{dt} \tag{14}$$

Applying Laplace transform to Eq. (25), the controller action is expressed in terms of the transfer function as:

$$C(s) = \frac{U(s)}{E(s)} = K_P + \frac{K_I}{s} + K_D\, s \tag{15}$$

where, $C(s)$ is the controller transfer function,$E(s)$ is the error, $U(s)$ is the output, K_P,K_I,K_D are the controller proportional, integral, and derivative gains.

Generally, when combined, these parameters will provide significant advantages in many applications. For example, the proportional control can produce a fast response, the integral control can eliminate the steady-state error, and the derivative control can increase the system's stability by reducing the overshoot and settling time. In this paper, PID can work as both a system and a force-tracking controller.

5.2 Optimization Algorithms

5.2.1 Ziegler-Nichols (Z-N) method

To tune the PID parameters, firstly, the Z-N method proposed has been implemented, which comes under rule-based methods. The tuning rules of PID using Z-N are very simple, providing good controller parameter values. Here, the step response of the plant assumes to have an S-shaped curve, as shown in Figure 6. From the curve, depending upon the value of L and T, a set of tuning parameters are established as given in Table 3, where L denotes the delay and T can be interpreted as the time constant calculated from the intersection of the tangent line with time axis and with the final value of the response, respectively.

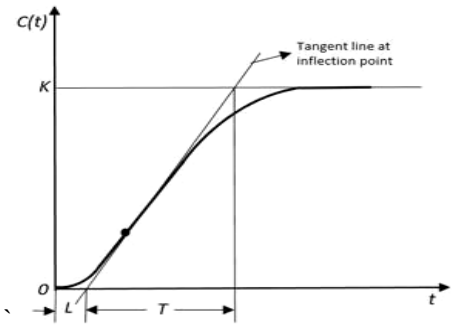

Figure 6. S-shaped step response of the system

Table 3. Gain parameters calculated usingthe Z-N method

Controller	K_P	T_i	T_d
P	$\frac{T}{L}$	∞	0
PI	$0.9\,\frac{T}{L}$	$\frac{L}{0.3}$	0
PID	$1.2\,\frac{T}{L}$	$2L$	$0.5L$

The parameters obtained from these rules can be used as a good initial guess for the metaheuristic optimization algorithms discussed below.

5.2.2 Particle Swarm Optimization

In recent years, the PSO algorithm has emerged as a potential tool for solving a wide range of problems in control engineering. The PSO algorithm uses the nature-inspired mechanism of bird flocking or fish schooling with a targeted position in searching for potential food. Kennedy et al. [41] proposed this algorithm in 1995, which uses the actions of swarm intelligence in which each particle focuses on finding the potential solution according to the given objective function. Each particle reaches its best position according to its own experience and awareness of the neighboring particle they are going through. Due to its diverse nature, such as by changing its parameters and population size, PSO can be easily used in conjunction with other heuristic algorithms. It uses in various kinds of applications, including financial studies [69], structural studies [70], electrical engineering [71], and automatic control systems [72]. In the control system, PSO is used mainly to solve the single or multi-objective function, which helps to get the desired transient and steady-state responses. The present investigation employed this algorithm to solve a single objective multivariable optimization problem using for proposed vibration control structure. The working flow diagram of this algorithm for the presently investigated problem is shown in Figure 7(a).

5.2.3 Ant Colony Optimization

Ant colony optimization is a population-based algorithm that can be used to find the approximate solutions to Mathematical and Engineering problems. Marico Dorigo proposes ACO in the 1990s [42]. It is inspired by the foraging behavior of ant colonies whose goal is to find the shortest path from their nest to their food source. Ant leaves a chemical compound called pheromone that helps communicate with other ants. When an ant finds food, it carries as much of it as possible. When it returns, it leaves a pheromone on the paths based on how much and how well it ate. Ants can smell pheromones. So other ants can smell it and go in that direction. The higher the level of pheromone, the more likely it is that the ant will take that path, and the more ants that take that path, the more pheromone will be on that path.In other words, an ant who travels a shorter distance to a food source will return to the nest sooner. The probability equation for the ant move from *i* to *j* node is expressed as:

$$p_{i,j} = \frac{\left(\tau_{i,j}^{\alpha}\right)\left(\eta_{i,j}^{\beta}\right)}{\sum\left(\tau_{i,j}^{\alpha}\right)\left(\eta_{i,j}^{\beta}\right)} \tag{16}$$

where, $\tau_{i,j}$= amount of pheromone on edge *i, j*, α= parameter to control the influence of $\tau_{i,j}$, $\eta_{i,j}$= Desirability of edge *i, j*, β= parameter to control the influence of $\eta_{i,j}$

There are various fields where ACO has successfully implemented to get the desired responses. These include the stabilization of the quadrotor [73], control of the human heart [74], load frequency control of nuclear power station [75], motor control of robotic arm[76], autonomous underwater vehicle [77], etc. This paper uses the ACO to tune the PID controller for vibration control application. The working flow diagram of this algorithm for the presently investigated problem is illustrated in Figure 7(b).

5.2.4 Flow Direction Algorithm

The flow direction algorithm is a newly metaheuristic optimization algorithm based on a physics-based algorithm. FDA was introduced by Hojat Karimi et al. [78]. It is inspired by the flow direction of the outlet point with the lowest height, achieving the optimal solution in the drainage basin. It utilizes the T8 method to find the flow direction in multi-dimensional search space.Here, the direction of runoff flows toward the outlet determines the solving pattern. In a basin, the natural phenomenon of flow moving to a position with the lowest high is the basis of the search algorithm. After filling the sink, the slope at which it moves mimics the escaping nature of the algorithm from local minimum points. The performance of this algorithm has been tested only against the benchmark function and other applications, such as data clustering [60] and energy harvesting in the paper industry. However, it is also imperative to observe the performance of this algorithm toward such real-time dynamic optimization problems. Hence, in this paper, we proposed this algorithm to tune the PID parameters, which control the suspension system of railway vehicles. The various steps of the FDA to find the optimal solution are illustrated below, and the working flow diagram of proposed algorithm is illustrated in Figure 7(c).

Steps of FDA:

1) Generating the initial population or flows.
2) Calculate the objective function and consider the best objective function as the outlet point.
3) Creating α number of neighbors with a neighborhood radius of Δ for each individual of the population or flows.
4) Specify the objective function value for each neighbor and determine the best neighbor.
5) If the best neighbor has a better objective function than the current flow, step VI should be implemented; otherwise, step VII is taken.
6) Update the flow velocity vector and generate a new position of the flow. Update the flow velocity vector and generating a new position of the flow.
7) Update the positions of flow.

8) Evaluate the objective function of new flows and update the objective function and position of the flows if it is better than previous flows.

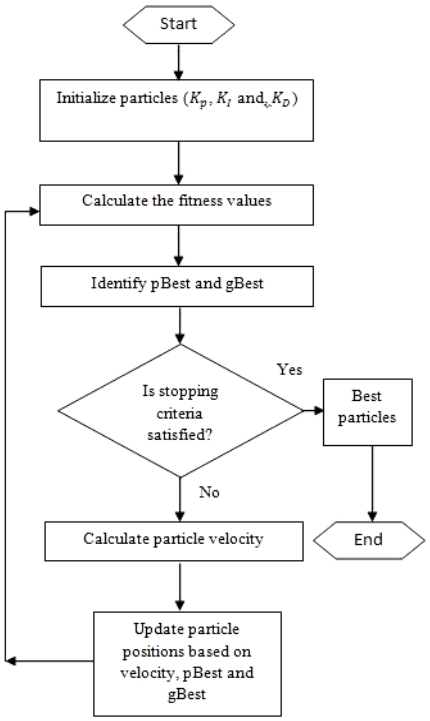

(a)

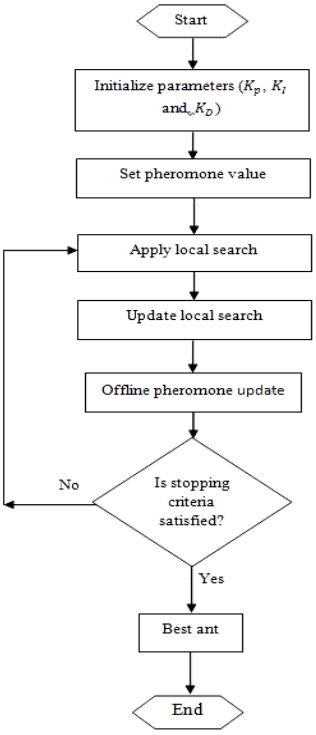

(b)

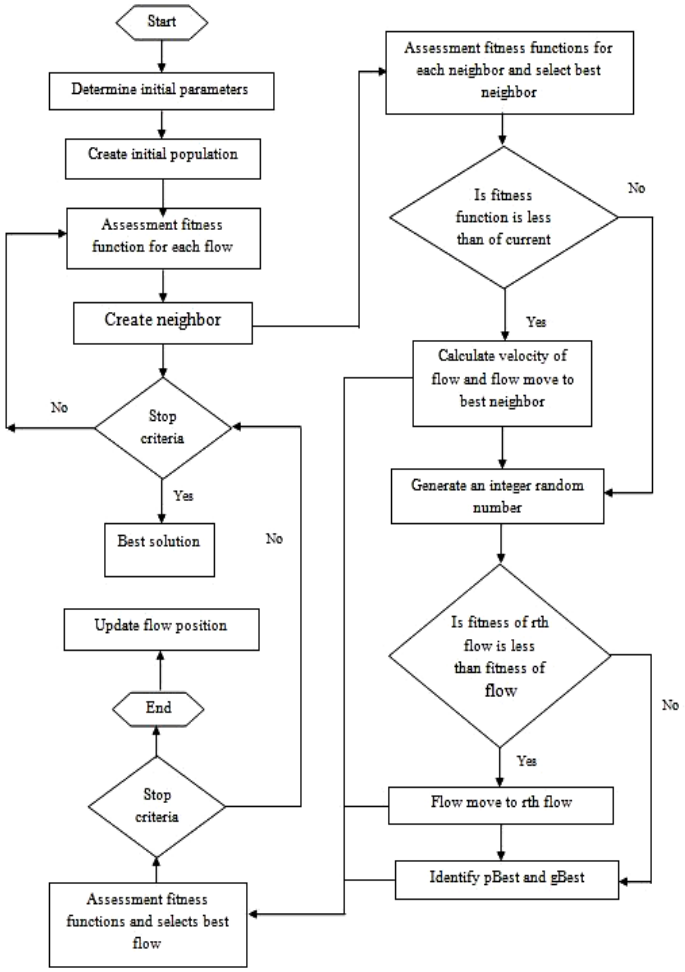

(c)

Figure 7. Flow chart of optimization algorithm: (a) PSO, (b) ACO and (c) FDA

6.0 SYSTEM RESPONSE BASED ON SYSTEM CONTROLLER

In order to achieve better ride comfort, the acceleration response of the vehicle body in translational as well as rotational motion should be minimized. Thus, from matrix [C] the controlled outputs $y = y_1$ are defined as:

$$[y_1] = [\ddot{Y}_c, \ddot{\psi}_c, \ddot{\Theta}_c] \tag{17}$$

Since the time lag between the first and last set of wheel-sets is much less for a high-speed railway. Therefore, let:

$$[w] = [Y_a, \theta_{cl}, \dot{Y}_a, \dot{\theta}_{cl}]^{\mathrm{T}} \cong [Y_{a1}, \theta_{cl1}, \dot{Y}_{a1}, \dot{\theta}_{cl1}, Y_{a2}, \theta_{cl2}, \dot{Y}_{a2}, \dot{\theta}_{cl2}, Y_{a3}, \theta_{cl3}, \dot{Y}_{a3}, \dot{\theta}_{cl3}, Y_{a4}, \theta_{cl4}, \dot{Y}_{a4}, \dot{\theta}_{cl4}]^{\mathrm{T}} \tag{18}$$

The single loop control structure of the MIMO system is shown in Figure8. In which Figure 8(a) represents the complete form of a single loop used to control one motion; correspondingly, the simplified form of this loop is shown in Figure 8(b).

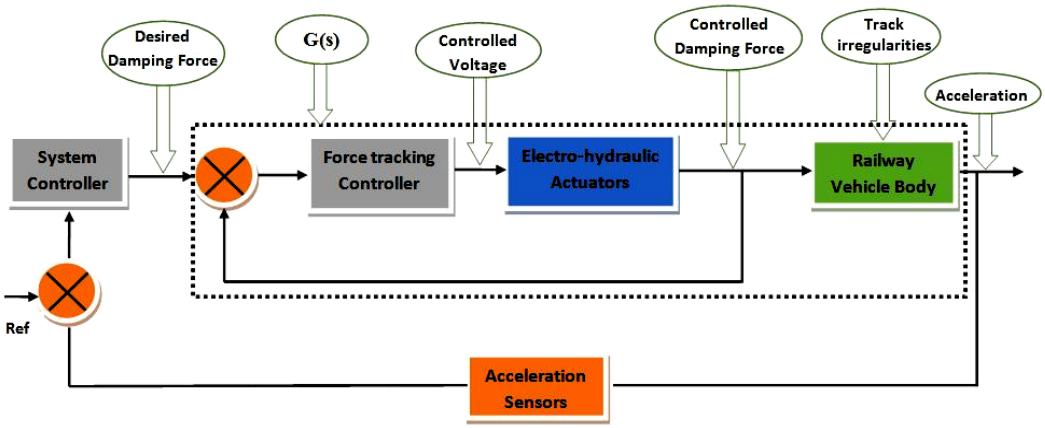

(a)

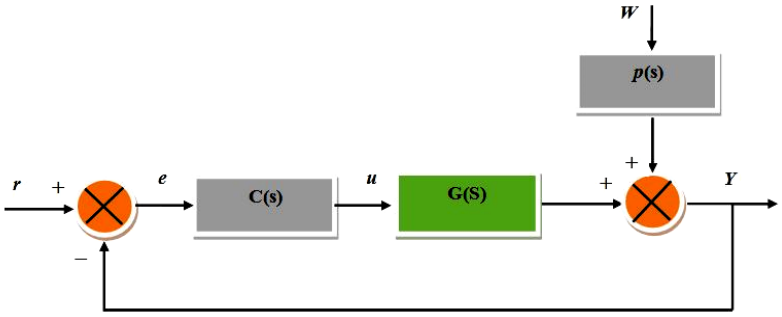

(b)

Figure 8. Single loop structure of regulatory feedback system

Thus, from Eqs. (10), (17), and (18), the two transfer function matrix, i.e., between the inputs (disturbance and control) and outputs of the system, can be evaluated as:

$$P(s) = \begin{bmatrix} p_{11}(s) & \cdots & p_{1n}(s) \\ \vdots & \ddots & \vdots \\ p_{n1}(s) & \cdots & p_{nn}(s) \end{bmatrix}; \quad G(s) = \begin{bmatrix} g_{11}(s) & \cdots & g_{1n}(s) \\ \vdots & \ddots & \vdots \\ g_{n1}(s) & \cdots & g_{nn}(s) \end{bmatrix} \tag{19}$$

where, $[P(s)]^{n\times n}$ represents the disturbance transfer function matrix having$n$ no. of disturbance inputs and n no. of outputs, and $[G(s)]^{n\times n}$ is a system transfer function matrix having n no. of control inputs and n no. of outputs.

Now, for a $n \times n$ control system, the transfer function matrix for the decentralized controller can be represented as:

$$C(s) = \frac{U(s)}{E(s)} = \begin{bmatrix} c_{11}(s) & 0 & \cdots & 0 \\ 0 & c_{22}(s) & \cdots & 0 \\ \vdots & \vdots & \vdots & \vdots \\ 0 & 0 & \cdots & c_{nn}(s) \end{bmatrix} \tag{20}$$

For the single-loop structure of the regulatory feedback system shown in Figure 7(b), the closed-loop transfer function between the input and output is:

$$\mathrm{T(s)} = \frac{Y(s)}{W(s)} = [1 + p(s)c(s)g(s)]^{-1}p(s) \tag{21}$$

Likewise, the overall transfer function matrix of the decentralized control system can be written as follows:

$$H(s) = diag[(1 + p_{11}(s)c_{11}(s)g_{11}(s)]^{-1}p_{11}(s)); (1 + p_{22}(s)c_{22}(s)g_{22}(s)]^{-1}p_{22}(s)) ; \dots\dots\dots\dots; (1 + p_{nn}(s)c_{nn}(s)g_{nn}(s)]^{-1}p_{nn}(s))] \quad (22)$$

Now, if $H_{nn}(\omega)$ is considered as frequency response function due to harmonically varying input of unit amplitude having frequency response function $W_n(\omega)$ for n^{th} input with all other input kept at zero. Then output and input of the system in the frequency domain are related by the relation as

$$Y_n(\omega) = H_{nn}(\omega) \times W_n(\omega) \quad (23)$$

In the case of random input, the input is considered in terms of PSD, as stated above in Eqs. (11) and(12). Then the output mean square spectral density $S_y(\omega)$ is related to the input mean square spectral density$S_n(\omega)$ as stated

$$S_y(\omega) = |H_{nn}(\omega)|^2 \times S_n(\omega) \quad (24)$$

where,

$$H_{nn}(\omega) = \frac{1}{1 - \left(\frac{\omega}{\omega_n}\right)^2 + j2\zeta_n\left(\frac{\omega}{\omega_n}\right)} \quad (25)$$

where $\left(\frac{\omega}{\omega_n}\right)$ is the normalized frequency and ζ is the damping ratio.

Then finally, the root mean square acceleration response is calculated as:

$$a_0 = \sqrt{\frac{1}{\pi}\int_{\omega 1}^{\omega 2} \omega^4 . S_n(\omega) d\omega} \quad (26)$$

7.0 RESULTS AND DISCUSSIONS

This section evaluates the performance of the PID-based active suspension control system used for vibration control of railway vehicles. The effectiveness of the controller tuned with metaheuristic optimization algorithms was investigated in the frequency domain under random track disturbances. The results are characterized in terms of power spectral densities. A comparison was conducted between the proposed PID control with the Z-N, PSO, ACO, and FDA tuning strategies. The improvement of proposed control schemes over the passive system was evaluated based on the following proposed linear quadratic regulator cost function.

$$J = \frac{1}{2}\int_0^{t_f} r_1 . x_{1\,max}^2 + r_2 . x_{2\,max}^2 \quad (27)$$

where $r_1$andr_2 represent the maximum accelerations and control efforts required for the respective state. According to the cost function, the lateral, roll, and yaw motion can be regulated by changing the values of the coefficientsw_1 (m/s^2), andw_2(N). The appropriate choices of the coefficients for translational and angular motions are as follows: r_1= 0.5, r_2= 2000. The various parameters of a railway vehicle (with loaded body mass) and track used in this study have been given in [22]. The simulation has been done in MATLAB/SIMULINK environment with a maximum step size of 1e-3.

The performance of an optimization-based PID controller depends on how well the controller parameters are tuned within the constraints of the required objective function, which ultimately depends on the values of controller parameters. Thus, by taking the classical approach (Z-N) as training optimum parameters, this method can provide an excellent initial guess for controller parameters and be a benchmark in designing the PID with the other metaheuristic techniques.Each algorithm has been run ten times by setting the same number of iterations, particles, and other parameters. Then, the best convergence graphs to find the optimum values of the PID controller using these techniques have been given in Figure. 9. Also, the best optimum PID parameters (K_p, K_p, K_p), and the corresponding cost function (O_f) values for lateral, roll, and yaw motion, results from classical and metaheuristic tuning, have been provided in Table 4. According to Figure 9, it is observed that although the convergence rate of PSO and ACO is substantially faster than the FDA, they are trapped in local minima, as demonstrated in Figures 9(a) and (b) do not guarantee an optimum solution. On the other hand, despite the rate of convergence of FDA being slower than PSO, ACO; still performs better for minimization of the cost function (O_f) as illustrated in Table 4, and also does not have the problem of getting trapped into local minimum points, which shows the efficacy of the proposed algorithm over PSO and ACO.

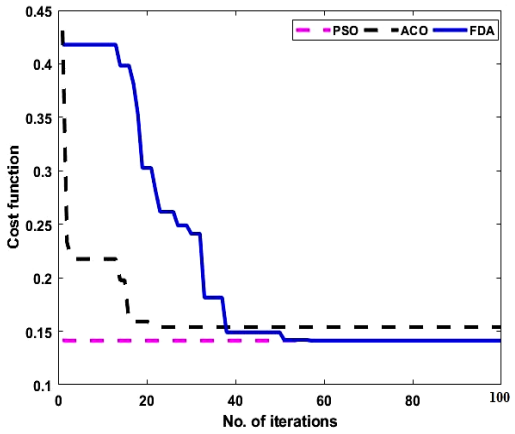

(a)

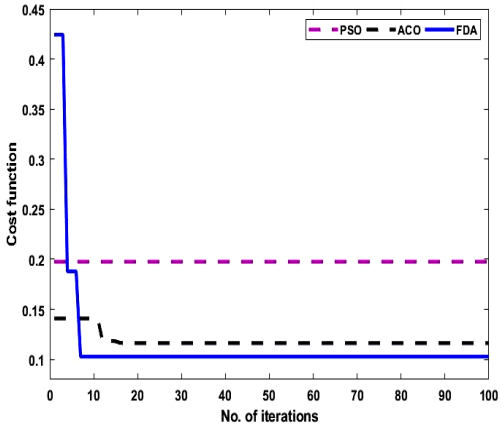

(b)

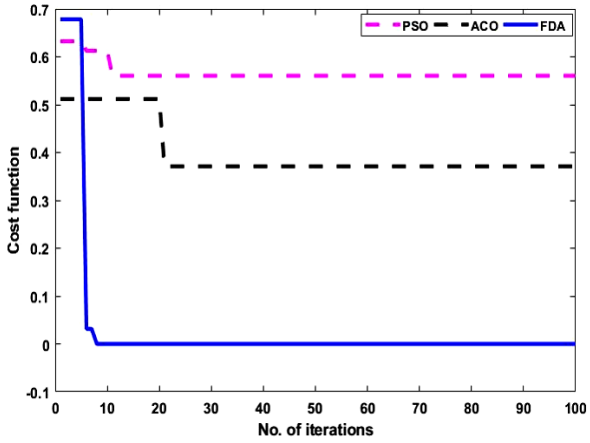

(c)

Figure 9. Convergence curves for: (a) lateral, (b) roll, and (c) yaw motions

Table 4. PID parameters and cost function values resulted from different tuning algorithms

(a) For lateral motion				
index	K_P	K_D	K_I	O_f
Z − N	4.256e-03	2.801e-03	1.064e-03	-
PSO	2.516e-03	3.453e-03	3.224e-03	0.147
ACO	2.072e-03	1.273e+03	0.626e-03	0.152
FDA	6.273e-02	7.736e-02	8.635e-03	0.143
(b) For roll motion				
index	K_P	K_D	K_I	O_f
Openloop	-	-	-	-
Z − N	1.873e-03	4.403e-03	2.463e-03	-
PSO	2.251e-03	3.516e-04	8.557e-4	0.197
ACO	2.982e-03	3.057e-03	4.560e-03	0.132
FDA	4.684e-02	8.362e-02	5.122e-02	0.033
(c) For yaw motion				
index	K_P	K_D	K_I	O_f
Open loop	-	-	-	-
Z − N	4.205e-04	3.011e-04	1.836e-04	-
PSO	2.056e-05	4.773e-04	4.263e-04	0.577
ACO	1.026e-03	3.544e-03	1.884e-03	0.382
FDA	4.835e-03	8.272e-03	5.021e-03	0.018

8.0 SIMULATION RESULTS

8.1 Frequency Domain Responses of Acceleration of the Body

To illustrate the efficiency of an optimally tuned PID controller in the frequency domain, two types of random track excitations (lateral alignment and cross-level) that act together have been considered as input. Using Eq. (24), the power spectral densities of the vehicle body's lateral, roll, and yaw accelerations of the open loop and closed loop control systems have been evaluated and are given in Figure 10. Also, the root means square values and the percentage improvement of RMS value of lateral, roll, and yaw acceleration over the passive system (open loop) are given in Table 6. The percentage improvement of RMS values using different tuning algorithms over the passive system has been calculated by using the following equation:

$$\%\ \text{improvement of RMS} = \frac{p_s - c_s}{p_s} \times 100 \tag{28}$$

where p_s and c_s are the RMS values of the passive and different PID-tuned control systems, respectively.

Until specified otherwise, the results we discussed below compare the three metaheuristic algorithms, PSO, GWO, and FDA, not with the classical tuning approach, i.e., Z-N. In the case of vertical motion, Figure 10(a) shows that the PID controller effectively reduces the two resonant peaks of lateral acceleration tuned with all three metaheuristic algorithms. However, among metaheuristic algorithms, FDA performs better in attenuating the lateral vibration at the range (0-20) rad/s. Also, the % improvement of lateral acceleration with the FDA algorithm over the passive system is 42.01%, which is comparatively higher than that of other optimization algorithms, as shown in Table 5(a). Observing Figure 10(b), it can be seen that the resonant peaks of roll acceleration are most successfully attenuated with the active suspension system tuned with FDA, as it can able to reduce the lateral vibration up to 33.12%, which is more than that of other tuning algorithms as rendered in Table 5(b).

From Figure 10(c), it is observed that the resonant peak of yaw acceleration at the range (0 -18) rad/s is successfully reduced with a suspension system controlled by an optimally-tuned PID controller, where the proposed FDA algorithm dominates the other tuning methods. The dominance of the PID controller with a hybrid algorithm over PSO and ACO is also verified in Table 5(c), where we can see that the suspension system tuned with the FDA can reduce the vibration level up to 48.24%, which is the highest among all the tuning algorithms.

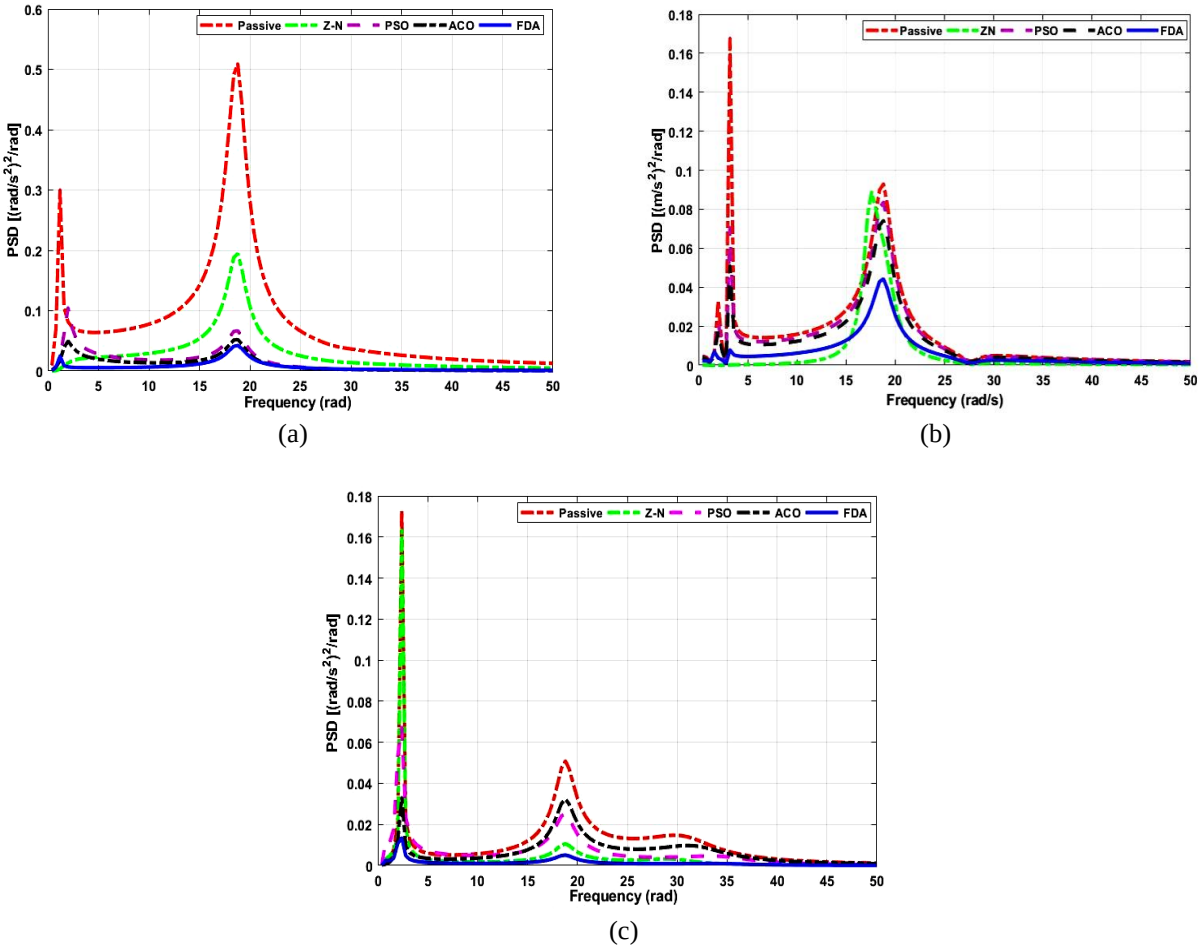

Figure 10. Power spectral densities of vehicle body acceleration under random track inputs (a) lateral acceleration) (b) roll acceleration and (c) yaw acceleration

Table 5. RMS, 'g' values and % improvement of vehicle body acceleration under random track disturbances

(a) For lateral motion					
index	Open-loop	Z-N	PSO	ACO	FDA
RMS Values	3.142e-03	2.552e-03	2.182e-03	1.895e-03	1.822e-03
'g' values	3.142e-04	2.552e-04	2.182e-04	1.895e-04	1.822e-04
% improvement	-	18.77 %	30.55 %	39.68 %	42.01 %
(b) For roll motion					
index	Open-loop	Z-N	PSO	ACO	FDA
RMS Values	2.221e-03	1.712e-03	1.430e-03	1.124e-03	0.823e-03
'g' values	2.221e-04	1.712e-04	1.430e-04	1.124e-04	0.823e-04
% improvement	-	12.11 %	18.73 %	25.98%	33.12 %
(c) For yaw motion					
index	Open-loop	Z-N	PSO	ACO	FDA
RMS Values	2.532e-03	1.901e-03	1.421e-03	1.142e-03	0.828e-03
'g' values	2.532e-04	1.901e-04	1.421e-04	1.142e-04	0.828e-04
% improvement	-	17.86 %	31.45 %	39.34 %	48.24%

The time histories of the acceleration of the vehicle body`s motions under random track irregularities have been shown in Figure 11. Figure 11 shows that the improvement of car body acceleration in all three modes using the active suspension system shows better attenuation than the passive system. It is worth noting that the reduction in acceleration amplitude using all three optimization techniques is very close to each other. Among them, the proposed algorithm FDA used to tune the PID parameters shows better vibration isolation than PSO and ACO.

Moreover, the time histories of controlling force given by the hydraulic actuator used to control the car body accelerations under random track irregularities have also been shown in Figure 12. Figure 12 shows that with the optimum tuning of the system controller with metaheuristic algorithms, the force-tracking ability of PID is also improved. It can track the desired force in the optimum range according to the proposed cost function. However, among all metaheuristic algorithms, FDA proves that it can follow the command force as closely as possible. From the simulation results shown and discussed in this section, it is observed that the improvement of acceleration of the vehicle body in all three modes using the PID controller tuned with three metaheuristic algorithms is remarkable as compared to the passive system and Z-N tuning approach. It is also noticeable that among the three metaheuristic algorithms, the controller tuned with the proposed FDA provides better attenuation than the controller tuned with the other two metaheuristic algorithms.

The performance of the proposed model also shows better results, as reported by previous research [7, 34, 79, 80], where the RMS reduction of the vehicle body is than 30 %. Therefore from these observations, we can say that the ride quality of railway vehicles with active suspension systems controlled with an optimal tuned PID controller is significantly improved compared to the passive system.

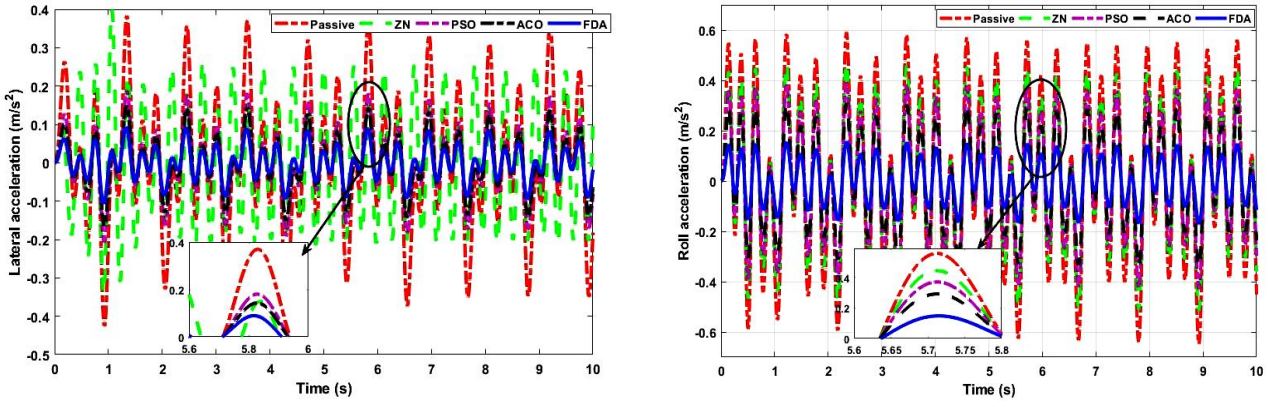

(a) (b)

Figure 11. Time histories of vehicle body acceleration under periodic track disturbances (a) lateral acceleration, (b) roll acceleration

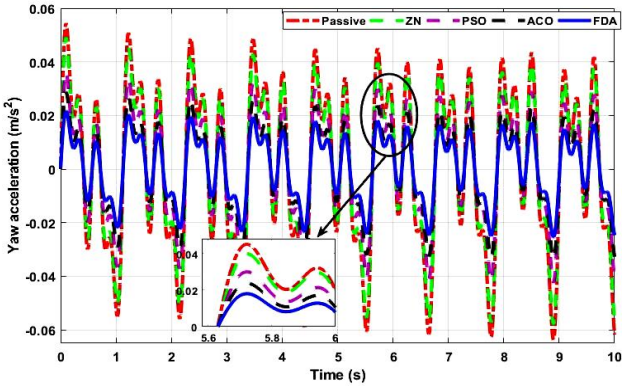

(c)

Figure 11. (cont.) (c) yaw acceleration

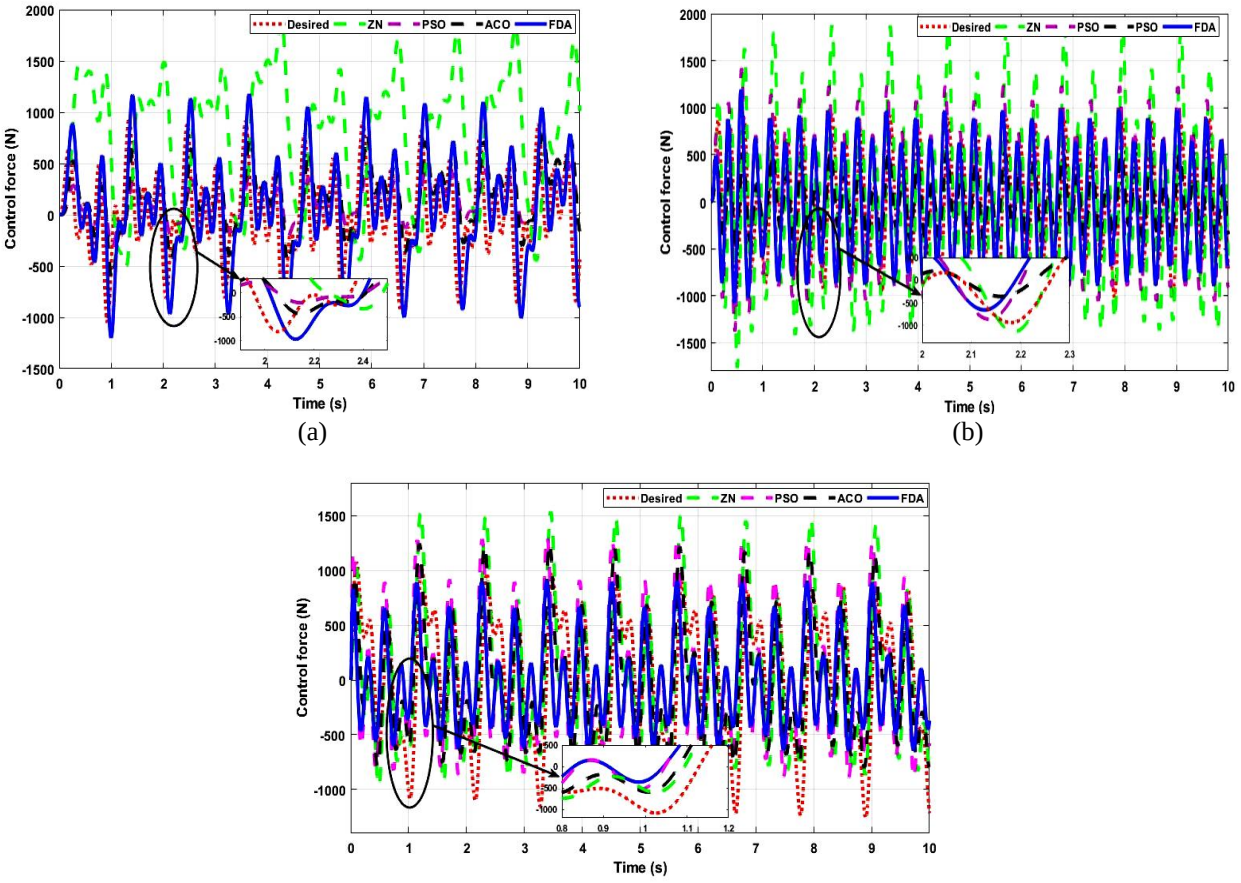

(a) (b)

(c)

Figure 12.Time histories of active force for different motions of a railway vehicle: (a) lateral motion, (b) roll motion and (c) yaw motion

9.0 VALIDATION OF RESULTS WITH EXPERIMENTAL DATA

The results of the proposed analytical model of LHB coach with passive and active suspension (tuned with different optimization) are validated using the oscillations test results. In particular, Research Design and Standard Organization conducted the test trials on a prototype Linke-Hofmann-Busch chair car to evaluate the acceleration and ride comfort in a test speed range of 33.33–55.55 m/s (120–200 km/h). The acceleration values have been evaluated using the coil and air springs as secondary suspensions. In the measurement, accelerometers and displacement sensors are connected by a cable to the data acquisition system in the equipment cabin. During oscillation test trials, these sensors capture acceleration and displacement signals on the axle box of the wheelsets, the car's floor, and the test coach's bogie frame. The experimental and simulated results of acceleration in the lateral directions at the speed of 200 km/h (55.55 m/s) have been compared, as shown in Figure 12**.** From Figure 13(a) and (b), it should be noted that the values of accelerations produced using the simulated model show a significant agreement with the experimental data of lateral acceleration. Figure 13

shows that the active suspension system controlled by metaheuristic-based PID improves ride comfort compared to the passive system.

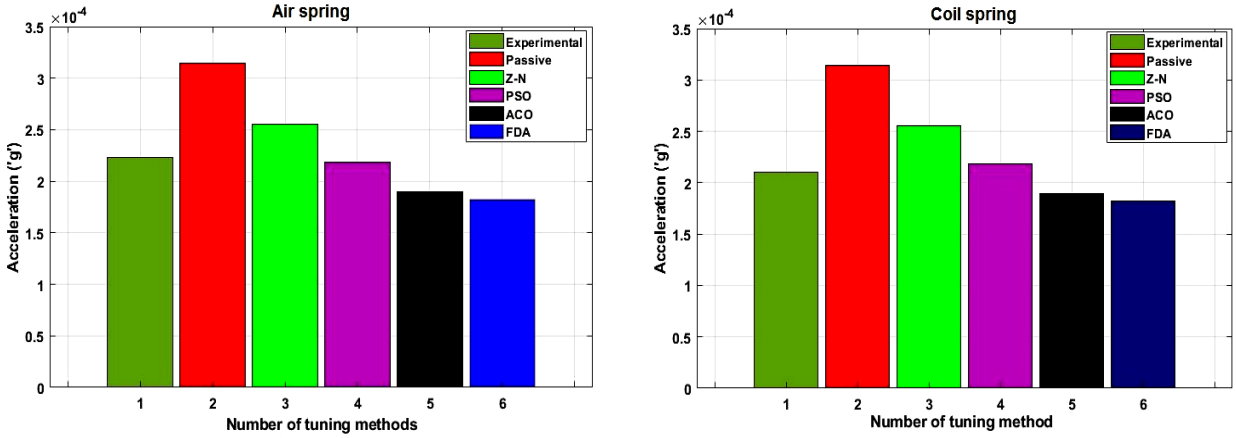

(a) (b)

Figure 13. Comparison of simulated results of lateral acceleration with experimental data in case of (a) air spring and (b) coil spring

10.0 CONCLUSIONS

In this paper, an active suspension system controlled by an optimal tuned PID controller is proposed to reduce the translational and angular vibrations of the car body. A 17-DOF dynamic model of a full-scale railway car with wheel-rail forces and active suspension was developed. After the development of the dynamic model, a decentralized control structure with three independent optimally tuned PID controllers, named system controllers, was utilized to estimate the desired force. Then, an electro-hydraulic-based suspension system was used to suppress the vibration of the car body. A new optimization method termed FDA was suggested to determine the optimum force for the suspension system. The simulated results were compared with a passive system and two other metaheuristic tuning algorithms (PSO, ACO). The car body's lateral, roll, and yaw accelerations under random track irregularities were investigated in frequency domains in the form of PSDs. According to simulation and analysis, the proposed optimization algorithm-based PID provides a good trade-off between maximum acceleration and control effort. But the controller tuned with FDA provides the best solution for the proposed cost function. The results show that the PID controller tuned with metaheuristic algorithms better suppresses resonant peaks over a wide range of frequencies. The superiority of the proposed controller is also verified as it can reduce the lateral, roll, and yaw acceleration up to 42.01 %, 33.12 %, and 48.24 %, respectively, compared to the passive system. Moreover the simulated acceleration results were compared against the experimental data to prove the validity of the proposed work. The comparison shows that the proposed system's results show a more significant agreement with the experimental data. Therefore, from the above discussions, it is clear that the ride quality of railway vehicles with active suspension systems tuned with metaheuristic algorithms is superior to those of railway vehicles with passive suspension systems.However, among metaheuristic approaches, the flow direction algorithm provides the best optimum results compared to particle swarm and ant colony optimization. In the future, the ride quality of railway vehicles could also be enhanced using a hybrid control structure tuned with a multi-objective cost function.

11.0 REFERENCES

[1] M. A. Karkoub and M. Zribi, "Active/semi-active suspension control using magnetorheological actuators,"*International Journal of System Science*, vol. 37, no. 1, pp. 35–44, 2006.

[2] L. R. Miller, "Tuning passive, semi-active, and fully active suspension systems," in *Proceedings of the 27th IEEE Conference on Decision and Contro*l, vol. 3, pp. 2047-2053, 1988.

[3] J. Rabinow, "The magnetic fluid clutch," *Transactions of American Institute of Electrical Engineering,* vol. 67, pp. 1308–1315, 1948,.

[4] W. Winslow, "Method and means for translating electrical impulses into mechanical force," *US Patent, 2417850*, 1947, [Online]. Available: http://www.freepatentsonline.com/2417850.html

[5] D. H. Wang and W. H. Liao, "Semi-active suspension systems for railway vehicles using magnetorheological dampers. Part I: System integration and modelling," *Vehicle System. Dynamics*, vol. 47, no. 11, pp. 1305–1325, 2009.

[6] X. Wei, M. Zhu, and L. Jia, "A semi-active control suspension system for railway vehicles with magnetorheological fluid dampers," *Vehicle System Dynamics*, vol. 54, no. 7, pp. 982–1003, 2016.

[7] L. H. Zong, X. L. Gong, S. H. Xuan, and C. Y. Guo, "Semi-active H∞ control of high-speed railway vehicle suspension with magnetorheological dampers," *Vehicle System Dynamics*, vol. 51, no. 5, pp. 600–626, 2013.

[8] X. Wu and M. J. Griffin, "A semi-active control policy to reduce the occurrence and severity of end-stop impacts in a suspension seat with an electrorheological fluid damper," *Journal of Sound and Vibration*, vol. 203, no. 5, pp. 781–793, 1997.

[9] S. B. Choi, J. H. Choi, M. H. Nam, C. C. Cheong, and H. G. Lee, "A semi-active suspension using ER fluids for a commercial vehicle seat," *Journal of Intelligent Material Systems and Structure*, vol. 9, no. 8, pp. 601–606, 1998.

[10] N. D. Sims and R. Stanway, "Semi-active vehicle suspension using smart fluid dampers: A modelling and control study," *International Journal of Vehicle Design*, vol. 33, no. 1–3, pp. 76–102, 2003.

[11] D. H. Wang and W. H. Liao, "Semi-active suspension systems for railway vehicles using magnetorheological dampers. Part II: Simulation and analysis," *Vehicle System Dynamics*, vol. 47, no. 12, pp. 1439–1471, 2009.

[12] B. Fu, E. Di Gialleonardo, B. Liu, and S. Bruni, "Modelling, hardware-in-the-loop tests and numerical simulation of magneto-rheological semi-active primary suspensions in a railway vehicle," *Vehicle System Dynamics*, 2023.

[13] M. M. ElMadany and M. E. Samaha, "On the optimum ride control of a stochastic model of a tractor-semitrailer vehicle," *Jounal of Sound and Vibration*, vol. 156, no. 2, pp. 269–281, 1992.

[14] B. Fu, R. L. Giossi, R. Persson, S. Stichel, S. Bruni, and R. Goodall, "Active suspension in railway vehicles: A literature survey," *Railway Engineering Science*, vol. 28, no. 1, pp. 3–35, 2020,.

[15] T. Yoshimura, K. Edokoro, and N. Ananthanarayana, "An active suspension model for rail/vehicle systems with preview and stochastic optimal control," *Journal of Sound and Vibration*, vol. 166, no. 3. pp. 507–519, 1993.

[16] D. Hrovat, "Optimal active suspension structures for quarter-car vehicle models," *Automatica*, vol. 26, no. 5, pp. 845–860, 1990.

[17] M. Metin and R. Guclu, "Rail vehicle vibrations control using parameters adaptive PID controller," *Mathamatical Problems in Engineeing*, vol. 2014, pp. 1-10, 2014.

[18] I. Afolabi Daniyan and K. Mpofu, "Vibration analysis and control in the rail car system using PID controls," *Noise and Vibration Control - From Theory to Practice*, IntechOpen, pp. 1–17, 2019.

[19] M. Metin and R. Guclu, "Active vibration control with comparative algorithms of half rail vehicle model under various track irregularities," *Journal of Vibration and Control*, vol. 17, no. 10, pp. 1525–1539, 2011.

[20] I. A. Daniyan, K. Mpofu, and D. F. Osadare, "Design and simulation of a controller for an active suspension system of a rail car," *Cogent Engineering*, vol. 5, no. 1, pp. 1–15, 2018.

[21] I. A. Daniyan, K. Mpofu, O. L. Daniyan, and A. O. Adeodu, "Dynamic modelling and simulation of rail car suspension systems using classic controls," *Cogent Engineering*, vol. 6, no. 1, pp. 1–20, 2019.

[22] Nitish and A. Kumar Singh, "Active control of railway vehicle suspension using PID controller with pole placement technique," *Materials Today: Proceedings*, vol. 80, pp. 278–284, 2023.

[23] S. Sezer and A. E. Atalay, "Dynamic modeling and fuzzy logic control of vibrations of a railway vehicle for different track irregularities," *Simulatiomn Modeling. Practice and Theory*, vol. 19, no. 9, pp. 1873–1894, 2011.

[24] R. Kalaivani, P. Lakshmi, and K. Sudhagar, "Vibration control of vehicle active suspension system using novel fuzzy logic controller," *International Journal of Enterprise. Network Management*, vol. 6, no. 2, pp. 139–152, 2014,.

[25] J. He, Z. Liu, and C. Zhang, "Sliding mode control of lateral semi-active suspension of high-speed train," *Journal of Advanced Computational Intelligence and Intelligent Informatics*, vol. 24, no. 7, pp. 925–933, 2020.

[26] S. B. Choi, Y. T. Choi, and D. W. Park, "A sliding mode control of a full-car electrorheological suspension system via hardware in-the-loop simulation," *Journal of Dynamic. Systems. Measurement and Control, Transactions of ASME*, vol. 122, no. 1, pp. 114–121, 2000.

[27] S. D. Nguyen and Q. H. Nguyen, "Design of active suspension controller for train cars based on sliding mode control, uncertainty observer and neuro-fuzzy system," *Journal of Vibration and Control*, vol. 23, no. 8, pp. 1334–1353, 2017.

[28] P. E. Orukpe, X. Zheng, I. M. Jaimoukha, A. C. Zolotas, and R. M. Goodall, "Model predictive control based on mixed H2/H∞ control approach for active vibration control of railway vehicles," *Vehicle System Dynamics*, vol. 46, no. .1, pp. 151–160, 2008.

[29] P. E. Orukpe, "Model predictive control application to flexible-bodied railway vehicles for vibration suppression," *International Journal of Engineering Research in Africa*, vol. 10, pp. 25–35, 2013.

[30] M. Olivier and J. W. Sohn, "Design optimization and performance evaluation of hybrid type magnetorheological damper," *Journal of Mechanical Science and Technology*, vol. 35, no. 8, pp. 3549–3558, 2021.

[31] M. Graa, M. Nejlaoui, A. Houidi, Z. Affi, and L. Romdhane, "Modeling and control of rail vehicle suspensions: A comparative study based on the passenger comfort," *Proceeding of the Institution of Mechanical Engineering, Part C: Journal of Mechanical Engineering Science*, vol. 232, no. 2, pp. 260–274, 2018.

[32] H. Molatefi, P. Ayoubi, and H. Mozafari, "Active vibration control of a railway vehicle carbody using piezoelectric elements," *Chinese Journal of Mechanical Engineering (English Edition)*, vol. 30, no. 4, pp. 963–972, 2017.

[33] D. Hrovat, "Applications of optimal control to advanced automotive suspension design," *Journal of Dynamic System Measurement and Control, Transactions of ASME*, vol. 115, no. 2B, pp. 328–342, 1993.

[34] Y. Shen, M. Jia, X. Yang, Y. Liu, and L. Chen, "Vibration suppression using a mechatronic PDD-ISD-combined vehicle suspension system," *International Journal of Mechanical Sciences*, vol. 250, p. 108277, 2023.

[35] T. Li, Y. He, N. Wang, J. Feng, W. Gui, and K. Zhao, "Active noise cancellation of rail vehicles based on a convolutional fuzzy neural network prediction approach," *IEEE Conference on Vehicle Power and Propulsion*, Gijon, Spain, 2021.

[36] I. Eski and Ş. Yildirim, "Vibration control of vehicle active suspension system using a new robust neural network control system," *Simulation Modeling Practice and Theory*, vol. 17, no. 5, pp. 778–793, 2009.

[37] V. S. Atray and P. N. Roschke, "Neuro-fuzzy control of railcar vibrations using semiactive dampers," *Computer-aided Civil and Infrastruct Engineering*, vol. 19, no. 2, pp. 81–92, 2004.

[38] K. J. Åström and T. Hägglund, "Revisiting the Ziegler-Nichols step response method for PID control," *Journal of Process Control*, vol. 14, no. 6, pp. 635–650, 2004.

[39] G. H. Cohenn and G. A. Coon, "Theoretical consideration of retarted control" *Transactions of ASME,* vol. 75, pp 827-834, 1953.

[40] A. E. Eiben, "Genetic algorithms + data structures = evolution programs," *Artificial Intelligence in Medicine*, vol. 9, no. 3. pp. 283–286, 1997.

[41] A. Slowik, "Particle swarm optimization," *The Industrial Electronic Handbook, Routledge Handbooks Online*, 2011.

[42] S. Mirjalili, "Ant colony optimisation," *Studies in Computational. Intelligence*, vol. 780, pp. 33–42, 2019.

[43] S. Mirjalili, S. M. Mirjalili, and A. Lewis, "Grey wolf optimizer," *Advances in Engineering Software*, vol. 69, pp. 46–61, 2014.

[44] S. L. Tilahun and H. C. Ong, "Modified firefly algorithm," *Journal of Applied Mathematics*, vol. 2012, pp. 1 - 12, 2012.

[45] X. S. Yang and S. Deb, "Cuckoo search via Lévy flights," *World Congress on Nature and Biological Inspired Computing (NABIC)*, Coimbatore, India, 2009.

[46] M. A. Al-Betar, M. A. Awadallah, I. Abu Doush, A. I. Hammouri, M. Mafarja, and Z. A. A. Alyasseri, "Island flower pollination algorithm for global optimization," *Journal of Supercomputing*, vol. 75, no. 8, pp. 5280–5323, 2019.

[47] A. T. El-Deen, A. A. Hakim Mahmoud, and A. R. El-Sawi, "Optimal PID tuning for DC motor speed controller based on genetic algorithm," *International Review of Automatic Control*, vol. 8, no. 1, pp. 80–85, 2015.

[48] N. F. Mohammed, E. Song, X. Ma, and Q. Hayat, "Tuning of PID controller of synchronous generators using genetic algorithm," *IEEE International Conference on Mechatronics and Automation*, Tianjin, China, 2014.

[49] A. G. Suri Babu and B. T. Chiranjeevi, "Implementation of fractional order PID controller for an AVR system using GA and ACO optimization techniques," *IFAC-PapersOnLine*, vol. 49, no. 1, pp. 456-461, 2016.

[50] D. H. Kim and J. Park, "Intelligent PID controller tuning of AVR system using GA and PSO," *Lecture Notes on Computational. Science*, vol. 3645, pp. 366–375, 2005.

[51] S. A. Adubi and S. Misra, "A comparative study on the ant colony optimization algorithms," *11th International Conference on Electronic. Computer and Computation (ICECCO)*, Abuja, Nigeria, 2014.

[52] R. J. Rajesh and C. M. Ananda, "PSO tuned PID controller for controlling camera position in UAV using 2-axis gimbal," *IEEE International Conference on Power and Advanced Control Engineering*, Bengaluru, India, 2015.

[53] S. B. Joseph, E. Dada, "Proportional-Intergral-Derivative Controller. tuning for an Inverted. Pendulum using particle swarm optimization algorithm," *FUDMA Journal of Science*, vol. 2, no. 2, pp. 72–78, 2018.

[54] M. Alamdar Ravari and M. Yaghoobi, "Optimum design of fractional order PID controller using chaotic firefly algorithms for a control CSTR system," *Asian Journal of Control*, vol. 21, no. 5, pp. 2245–2255, 2019.

[55] M. I. Mosaad, M. Osama abed el-Raouf, M. A. Al-Ahmar, and F. A. Banakher, "Maximum power point tracking of PV system based cuckoo search algorithm; review and comparison," *Energy Procedia*, vol. 162, pp. 117–126, 2019.

[56] M. Peram, S. Mishra, M. Vemulapaty, B. Verma, and P. K. Padhy, "Optimal PI-PD and I-PD controller design using cuckoo search algorithm," *5th International Conference on Signal Processing and Integrated Networks*, Noida, India, 2018.

[57] A. Sikander, P. Verma, N. Patel, and N. K. C. Nair, "Design of controller using reduced order modeling for LED driver circuit,". *IEEE Innovative Smart Grid Technology. - Asia (ISGT-Asia),* Auckland, New Zealand, 2018.

[58] S. X. Li and J. S. Wang, "Dynamic modeling of steam condenser and design of pi controller based on grey wolf optimizer," *Mathematical Problems in Engineering.*, vol. 2015, pp. pp. 1 - 9, 2015.

[59] S. Yadav, S. K. Verma, and S. K. Nagar, "Optimized PID controller for magnetic levitation system," *IFAC-PapersOnLine*, vol. 49, no. 1, pp. 778–782, 2016.

[60] L. Abualigah, K. H. Almotairi, M. A. Elaziz, M. Shehab, and M. Altalhi, "Enhanced flow direction arithmetic optimization algorithm for mathematical optimization problems with applications of data clustering," *Engineering Analysis with Boundary Elements*, vol. 138, pp. 13–29, 2022.

[61] S. Pati, T. Kumar Sharma, K. Kumar Goyal, and O. Prakash Verma, "Renewable integration and energy reduction in multiple stage evaporator," *Materials Today Proceedings*, vol. 80, pp. 24-31, 2022.

[62] Y. Luo, H. Liu, L. Jia, and W. Cai, "A practical guideline to control structure selection for MIMO processes," *IEEE International Conference on Automated Logistical*, Chongqing, China, 2011.

[63] M. J. Lengare, R. H. Chile, and L. M. Waghmare, "Design of decentralized controllers for MIMO processes," *Computers. and Electrical Engineering*, vol. 38, no. 1, pp. 140–147, 2012.

[64] Y. Lei and D. T. Wu, "A new decentralized control approach for the benchmark problem," *Procedia Engineering*, vol. 14, pp. 1229–1236, 2011.

[65] S. D. Singh, R. Mathur, and R. K. Srivastava, "Dynamic response of Linke Hofmann Busch (LHB) rail coach considering suspended equipments," *Indian Journal of Science and. Technology*, vol. 10, no. 38, pp. 1–20, 2017.

[66] M. J. Goodwin, "Dynamics of railway vehicle systems," *Journal of Mechanical Working Technology*, vol. 14, no. 2, pp. 245–247, 1987.

[67] M. A. A. Abdelkareem *et al.*, "Vibration energy harvesting in automotive suspension system: A detailed review," *Applied Energy*, vol. 229, pp. 672–699, 2018.

[68] C. Williamson, S. Lee, and M. Ivantysynova, "Active vibration damping for an off-road vehicle with displacement controlled actuators," *International Journal of Fluid Power*, vol. 10, no. 3, pp. 5–16, 2009.

[69] F. S. Shie, M. Y. Chen, and Y. S. Liu, "Prediction of corporate financial distress: An application of the America banking industry," *Neural Computing and Applications*, vol. 21, no. 7, pp. 1687–1696, 2012.

[70] M. Hajihassani, D. Jahed Armaghani, and R. Kalatehjari, "Applications of particle swarm optimization in geotechnical engineering: A comprehensive review," *Geotechnical and Geological Engineering*, vol. 36, no. 2, pp. 705–722, 2018.

[71] S. Ganguly, N. C. Sahoo, and D. Das, "A novel multi-objective PSO for electrical distribution system planning incorporating distributed generation," *Energy Systems*, vol. 1, no. 3, pp. 291–337, 2010.

[72] W. Der Chang and C. Y. Chen, "PID controller design for MIMO processes using improved particle swarm optimization," *Circuits, Systems and Signal Processing*, vol. 33, no. 5, pp. 1473–1490, 2014.

[73] T. K. Priyambodo, A. E. Putra, and A. Dharmawan, "Optimizing control based on ant colony logic for Quadrotor stabilization," *IEEE International Conference on Aerospace Electronics and Remote Sensing Technology (ICARES)*, Bali, Indonesia, 2016.

[74] M. Aabid, A. Elakkary, and N. Sefiani, "PID parameters optimization using ant-colony algorithm for human heart control," *23rd International Conference on Automation and Computing (ICAC)*, Huddersfield, United Kingdom, 2017.

[75] B. Dhanasekaran, S. Siddhan, and J. Kaliannan, "Ant colony optimization technique tuned controller for frequency regulation of single area nuclear power generating system," *Microprocessors and Microsystems*, vol. 73, p. 102953, 2020.

[76] S. A. Dahmane, A. Azzedine, and A. Megueni, "Ant colony optimization algorithm based on optimal PID parameters for a robotic arm," *International Journal of Control Syatems and Robotics*, vol. 5, pp. 8–13, 2020.

[77] T. K. Priyambodo, A. Dharmawan, O. A. Dhewa, and N. A. S. Putro, "Optimizing control based on fine tune PID using ant colony logic for vertical moving control of UAV system," *Advances of Sciences and Technology for Society*, vol. 1755, pp. 1 - 6, 2016.

[78] H. Karami, M. V. Anaraki, S. Farzin, and S. Mirjalili, "Flow Direction Algorithm (FDA): A novel optimization approach for solving optimization problems," *Computers and Industrial Engineering*, vol. 156, p. 107224, 2021.

[79] S. Singh and A. Kumar, "Modelling and analysis of a passenger train for enhancing the ride performance using MR-based semi-active suspension," *Journal of Vibration Engineering and Technology*, vol. 10, no. 5, pp. 1737–1751, 2022.

[80] H. Cao, G. Li, and N. Liang, "Active vibration control of railway vehicle car body by secondary suspension actuators and piezoelectric actuators," *IEEE Access*, vol. 10, pp. 105404–105411, 2022.